JOURNAL OF MATERIALS SCIENCE 28 (1993) 2013–2027

Fatigue-induced damage mechanisms in carbon fibre-reinforced plastic composites

A. S. CHEN, B. HARRIS‡
School of Materials Science, University of Bath, Bath, BA2 7BY, UK

A study has been made of the damage mechanisms introduced by the fatigue process in two high-performance carbon-fibre-reinforced plastic laminates, XAS/914 and T800/5245. A series of experiments has been carried out to evaluate systematically the fatigue damage mechanisms that occur at different cyclic stress levels during repeated tension loading. The state and development of damage were mainly investigated by means of edge replication. Microscopy studies were used in support of the non-destructive evaluation methods. Important information relating to the onset of various types of fatigue-induced damage is presented in the form of schematic "damage maps". When the differences in strength of the two materials are taken into account, it appears that the XAS system exhibits fatigue resistance superior to that of the T800 system.

1. Introduction

Advanced fibre-reinforced composite materials offer substantial advantages over metallic materials for engineering application in structures subjected to fatigue loading. With the increasing application of carbon-fibre-reinforced composites, for intelligent engineering design there is a fundamental requirement for an understanding of their response to cyclic loads. A major aspect of the development of this understanding is that of detecting how and when damage occurs under various service conditions, so as to know what effect this damage may have on the properties.

As a consequence of their inhomogeneous and anisotropic nature, fatigue damage in fibre-reinforced composites can occur in the form of matrix cracking, fibre/matrix debonding, delamination and localized fibre breakage, or various complex combinations of these. It is generally agreed that the mechanisms and distribution of damage depend on the material system, stacking sequence of plies, geometry, stress state, loading history and environmental conditions [1]. Up to this point, all effort in the investigation of damage development of carbon-fibre-reinforced plastic (CFRP) under cyclic loading can be basically divided into two approaches [2]. One approach is deductive, in which the development of theoretical models is according to macroscopic measurements or phenomenological observations. That is, to use experimental results to confirm a theoretical analysis based on classical macroscopic mechanics or energy theories [3–8], and to postulate damage modes [9, 10]. Final failure is predicted on the basis that one or more of these damage modes have developed to a certain critical or unstable condition from which failure follows in a certain manner. Several significant attempts of this kind have been made and such models are evaluated in terms of stiffness reduction [11–13], residual mechanical properties and fatigue life, etc. [14–16].

The other approach is that which attempts to set up a damage model based on the observation of microscopic damage development. The microstructural damage modes are viewed as primitive elements of a complete description in which global phenomena are explained in terms of microstructural damage states. This approach provides an opportunity directly to relate the macroscopic properties of the material to the damage modes which already exist in it. This approach includes work dealing with the role of matrix cracking [17–20], delamination [21], fibre breakage [22], and combinations of these [23], and also work dealing with the influences of external parameters, such as fatigue frequency [24–27] and environmental effects [28, 29], on the development of microstructural damage. Although both approaches have shown reasonable degrees of success [2], from a materials science point of view the latter is the more practical method because the damage mechanisms and the mechanical properties depend strongly on the material system. In other words, they depend on the microstructure of the material. The basic attribute of this approach is that a philosophy of failure of fibre-reinforced composites can only be generated on the basis of a complete understanding of the damage states which caused it. It is in this area, that the present work has been designed to make its own contribution.

‡Author to whom all correspondence should be addressed.

0022–2461

2. Experimental procedure

2.1. Materials

The main material used in the programme was a standard high-strength, intermediate failure strain, Courtauld XAS carbon fibre in BSL 913 epoxy resin composite system. This was supplied by Ciba-Geigy in zero-bleed prepreg form with a nominal fibre content of 66% by weight. A second variety of material used was the intermediate modulus Torayca T800 carbon fibre in BASF (Narmco) bismaleimide 5245 epoxy resin composite system which was also purchased as zero-bleed prepreg with 66% nominal fibre content by weight from BASF Narmco Materials. The stacking sequence of both materials was 16-ply $[(\pm 45, 0_2)_2]_s$, which contains major geometric elements of lay-up systems familiar in aerospace engineering applications. The laminates had a nominal cured thickness of 2 mm: the XAS/914 system was hot pressed and the T800/5245 system autoclaved, following the manufacturers' specifications. All of the test specimens were cut to dimensions of 200 mm long by 20 mm wide, straight-sided (unwaisted). The edges of the test coupons were smoothed by using abrasive paper to remove the visibly rough sawn surfaces, and then soft aluminium end-tabs were glued on to both ends of each test coupon. The edges of the specimens on which the edge replication technique would be applied were further polished. The basic tensile mechanical properties of the composite laminates are shown in Table I.

2.2. The edge replication technique

As edge replication of composite material specimens has been employed with considerable success in damage mechanism studies, it was chosen as a major non-destructive testing (NDT) method in this work. In order to apply the technique effectively, the specimens were polished to a degree suitable for metallographic examination. The replicas were made on strips of cellulose acetate tape, supplied by Bio-red Microscience. The strip was laid on a piece of glass microscope slide and softened with acetone before being pressed into contact with the edge of the specimen. After about half an hour to allow the evaporation of the solvent, the film, which retains a permanent replica of the edge topography, could be removed from the test sample for examination under an optical microscope without the need for shadowing with a metal film. A major advantage of this technique is that the chronology of edge damage history can be recorded without disturbing the fatigue testing arrangements. However, to detect damage inside the sample away from the edges and build up a reasonably complete picture of the damage state in the bulk of the sample, other damage detection methods are needed.

TABLE I Tensile mechanical properties of the CFRP laminates

Composite	Modulus (GPa)	Strength (GPa)	Failure strain (%)
XAS/914 $[\pm 45, 0_2)_2]_s$	80.18 ± 4.00	1.01 ± 0.04	1.26 ± 0.05
T800/5245 $[(\pm 45, 0_2)_2]_s$	89.68 ± 3.92	1.62 ± 0.09	1.68 ± 0.09

2.3. Methods

Fatigue tests were carried out in a pair of Instron series 1300 servo-hydraulic machines operating under load control by computers via SArGen (Signal Analysis and Generator) control and data acquisition systems built by Marandy Instruments of Bath. The SArGen-computer control system has the capability of driving the fatigue machine in load control mode from zero load to a full pre-determined loading level in just ten cycles. This fast setting ability has dramatically increased the countable accuracy in low-cycle ranges compared to conventional amplitude control, and provided an opportunity for us to investigate the damage mechanisms which occurred during the early stages of a fatigue process. It also allowed us to carry out the edge replication technique with minimum effect on the outcome of fatigue tests. All cyclic tests were run at 5–10 Hz in tension–tension mode, with the ratio of minimum stress to maximum stress, $R = 0.1$, in a constant amplitude sine-wave loading, under ambient laboratory conditions.

In the first stage of the programme, proof tests were carried out on sufficient numbers of the specimens to determine stress/log life (S/log N) curves for the materials, which provide guidance for the fatigue tests in the next stage. In the second stage, which is the core part of the programme, the damage mechanisms were studied at several different stress levels (given percentages of ultimate strengths). In the course of each fatigue test, the test was stopped at some pre-determined number of cycles for the application of the edge replication technique. Because the specimen remained clamped in the machine, the fatigue test conditions were retained by the computer controller for continuation of the replication test. The fatigue tests were finally stopped, either at the failure of a specimen or after a certain number of cycles. Most of the unbroken samples were kept for residual property measurements, the results of which will be reported in a separate paper. Some of the fatigued specimens were sectioned for microscopic studies. The sections were cut parallel to the edge of the test coupons, and at $\frac{1}{16}$, $\frac{1}{8}$, $\frac{1}{4}$ and $\frac{1}{2}$ of the width of the samples. The polished section surfaces were examined under an optical microscope with the objective of analysing the different damage states in relation to the distance from the edge of the specimen. An additional microstructural study has been carried out on a JEOL scanning electron microscope (SEM) in order to evaluate the fatigue damage mode at the level of the fibre and matrix interfacial bond.

3. Results

Results of fatigue life tests for all three laminates are presented in Fig. 1 as fatigue peak stress/log life curves (S/log N). Apart from the differences in the ultimate strengths, the S/log N curve for the XAS/914 system is

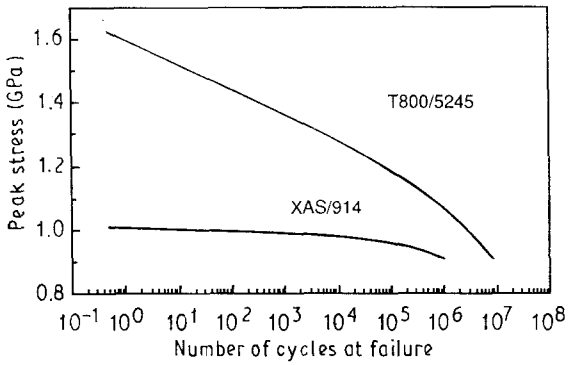

Figure 1 $S/\log N$ curves for XAS/914 and T800/5425 $[(\pm 45, 0_2)_2]_s$ laminates, $R = 0.1$.

much flatter than that for the T800/5245 system. All the curves have shown a tendency to tail off after about 10^5 cycles. The following mechanisms investigation has been carried out in the stress/life range within the $S/\log N$ curves indicated for the individual material systems.

3.1. XAS/914 $[(\pm 45, 0_2)_2]_s$ laminate

3.1.1. Damage mechanisms observed by edge replication

The edge replication technique permits detection of the damage state on the edges of specimens. As a result of the "free-edge effect", useful information on damage initiation and growth can be obtained by the technique. This strongly edge-related information will be supported by that which was obtained in the sectioning studies.

Fig. 2a–k show typical damage development recorded by edge replicas in a test coupon which was fatigued at a maximum stress equal to 94% of the monotonic ultimate strength. At a very early stage, after only 301 cycles, the first signs of damage, namely matrix cracks, appeared in an outer 45° ply (skin layer; Fig. 2a). At about the same time, fibre breakage in the 0° plies was observed (Fig. 2b). When the specimen was fatigued to 2512 cycles, matrix cracks occurred in the inner $\pm 45°$ plies (Fig. 2c), the number of matrix cracks continuing to increase in the outer 45° plies. After about 6800 cycles, fibre breakage spread throughout the 0° plies, and some broken fibre ends dropped out of the sample (Fig. 2d) from the edge of the specimen. Fig. 2e shows this at higher magnification. With further fatigue, the number of matrix cracks in the 45° plies increased, and edge delamination between two adjacent $\pm 45°$ plies appeared in all pairs of $\pm 45°$ plies (Fig. 2f). Although this edge delamination damage occurs along the whole boundary length at this stage, it started much earlier as several separate small edge delaminations as an appropriate stress condition was built up as a consequence of the presence of two matrix cracks in adjacent 45° plies (see Fig. 2c). The last damage mechanism which was observed in the edge replicas is delamination between the 0° and the 45° plies (Fig. 2g). This delamination could also start from approaching matrix cracks in adjacent 45° plies (Fig. 2h). In a few cases the opening matrix crack in a 45° ply could introduce a sufficiently high local normal stress concentration in the crack direction in the neighbouring 0° ply to trigger some fibre fractures as a continuation of the crack across the boundary into the 0° layer (Fig. 2i). This kind of crack will then be prevented from further growth by the formation of new matrix cracks between the fibres and parallel to the boundary. Fig. 2j is a picture of the last replica taken from this specimen which then failed after a further 542 cycles in the fatigue test.

Fig. 3a–g record the damage initiation and development on the edge of another specimen which was fatigued at a peak stress of 78% of the ultimate strength. Despite the different numbers of cycles, they show a similar history of damage development to that described above. The outer matrix cracks were observed, along with fibre breakage, at about 8000 cycles (Fig. 3a and b) which was much later than in the previous case. Fig. 3c shows such a matrix crack in an inner 45° ply. Subsequently, the fibre drop-out mechanism occurs (Fig. 3d) from the free edge, together with delamination between adjacent $\pm 45°$ plies as a result of an increase of the number of matrix cracks (Fig. 3e) and delamination between 0° and 45° plies (Fig. 3f). This specimen did not fail up to 962 496 cycles, and Fig. 3g shows the last replica taken from this sample after cyclic loading had been terminated.

A total of 18 specimens which were cycled at maximum fatigue stress levels from 66% up to nearly 100% of the static strength was examined by this method. Apart from a few which were cycled at high stress, approximately 95% or above, and had quite short lifetimes, almost all of the others have exhibited all of the damage modes described above in different stages of their life. The replica information may be presented in the form of a damage mechanisms map in terms of peak fatigue stress versus number of cycles, as shown in Fig. 4 which also includes the $S/\log N$ curve.

3.1.2. Density of matrix cracks on sample edges

By counting the number of matrix cracks, it has been observed that there is a slowing down of the rate of initiation of the matrix cracks in both outer and inner 45° plies after certain levels of crack density are reached. Fig. 5a shows the rate of increase in the number of matrix cracks in the free edge of a specimen which was fatigued at a peak stress of 94% of the tensile strength, as shown in Fig. 2, in terms of density of cracks (the number of cracks per unit length in one 45° ply), versus logarithmic number of cycles. It can be seen that following a rapid initial increase the matrix crack densities in both outer and inner 45° plies were settling down to different constant levels. These constant crack density levels, about 2.4 per mm for outer 45° plies and 3.5 per mm for the inner plies, were not altered by changing the fatigue stress levels. Fig. 5b and c show the matrix crack densities observed in different samples fatigued at lower peak stress levels of 86% and 78% of the tensile strength, respectively, and the latter is the sample referred to in Fig. 3. Although

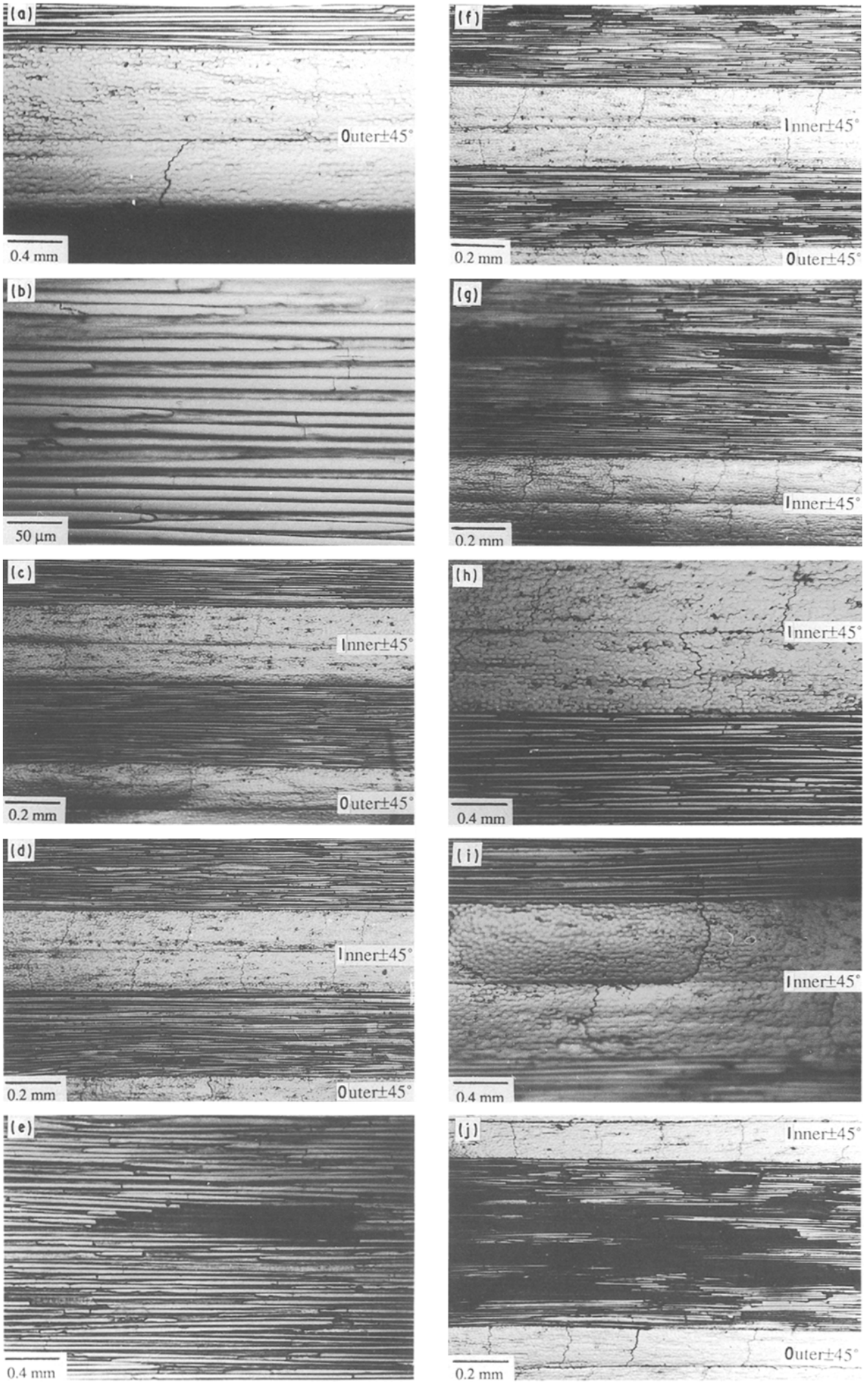
(a)
Outer±45°
0.4 mm
(b)
50 μm
(c)
Inner±45°
0.2 mm
Outer±45°
(d)
Inner±45°
0.2 mm
Outer±45°
(e)
0.4 mm
(f)
Inner±45°
0.2 mm
Outer±45°
(g)
Inner±45°
0.2 mm
(h)
Inner±45°
0.4 mm
(i)
Inner±45°
0.4 mm
(j)
Inner±45°
Outer±45°
0.2 mm

the point of initiation of matrix cracking during fatigue was delayed by applying lower peak cyclic loads, the rate of initiation of cracks still slowed down towards densities of about 2.4 and 3.5 mm^{-1} for the outer and inner $\pm 45°$ plies, respectively. This is the so-called "characteristic damage state" (CDS) in off-axis plies [17, 18], and was clearly present in this laminate at all test fatigue stress levels used in the experimental programme.

3.1.3. Microscopic examination of sample sections

Four samples which were fatigued at peak stresses of 75% and 86% of the tensile strength separately to 5×10^4 and 10^6 cycles were successively sectioned longitudinally at $\frac{1}{16}$, $\frac{1}{8}$, $\frac{1}{4}$ and $\frac{1}{2}$ of the width of the sample, parallel to the edge, and polished for optical microscopy. The most significant observation on these section surfaces, for all four samples, is that not all of the matrix cracks grow through the whole specimen width. The further away the section surface is from the free edge, the fewer matrix cracks can be observed. By counting the number of matrix cracks in all of the sectioned surfaces, the changes in the densities of matrix cracks with distance from the nearest free edge on the test samples can be determined, and these are plotted in Fig. 6a and b for two different stress levels. A clear reduction in the densities of matrix cracks in both outer and inner $\pm 45°$ plies at both stress levels has been observed. Having assumed that the cracks which were observed in the half-width section surface had passed through the whole width of the specimen, it can be seen that only about half the number of matrix cracks in the inner $\pm 45°$ plies penetrated the whole width of the specimens up to a late stage in the fatigue life-time, about 10^6 cycles at both stress levels, even though the matrix crack states on the free edges were already at or near the CDS.

The matrix cracks penetrate the outer 45° plies more easily as shown by the fact that the reductions in the matrix crack densities with distance into the samples are smaller in these than in the inner plies, except in one very low-density case, for the lower stress level in an early fatigue stage. And the actual numbers of cracks in these skin plies are also less than in the inner 45° plies, despite the early fatigue life, lower stress level case again. Because the thickness of the specimens is much smaller than their width, 2 mm/20 mm = 0.1, the stress distribution in the through-thickness direction is expected to be flatter or more uniform than in the width direction. As a result of such a flat stress distribution, the difference between the crack densities in the inner and outer plies on the same section surface, especially on the half-width section ones, is less significant than in the width direction.

The fibre drop-out mechanism that occurs on the free edges can also be seen in the cut sections. Fig. 7a and b are two pictures taken from half-width sectioned surfaces of two samples fatigued to 10^6 cycles at peak stress levels of 86% and 75% of the tensile strength, respectively. A missing group of fibres and a missing piece of fibre can clearly be seen in the photographs.

It has been found in the sectioning studies that the delamination is indeed very much edge-related. Fig. 8a and b show a set of pictures of the section surface at $\frac{1}{16}$ of the width of a sample (approximately 1.2 mm from the edge) which was fatigued to 10^6 cycles at 86% of the tensile strength. A continuous delamination can still be seen in both outer (Fig. 8a), and inner (Fig. 8b) $\pm 45°$ plies. On increasing the distance from the edge to $\frac{1}{8}$ of the width of the same sample (approximately 2.5 mm), the continuous delamination between the inner $\pm 45°$ plies no longer exists (Fig. 8c) even though that between the two outer plies can still be clearly seen (Fig. 8d). This corresponds well with the hypothesis that the width of the boundary layer affected by the free edge effect is of the same dimension as the laminate thickness [30, 31]. On further increasing the sectioning distance to a quarter (Fig. 8e and f) and a half of the width (Fig. 8g), only discontinuous delamination can be observed. And these small interlaminar cracks found in the deep section surface could be formed under the shear stress concentration caused by the conjunction of two in-ply matrix cracks in two adjacent $\pm 45°$ plies as interlaminar cracks, mainly in Modes II and III. A similar situation occurs in relation to the delamination between 0° and 45° plies. This delamination, observed in the edge replicas, grows much less deeply into the laminate than that between $+45°$ and $-45°$ plies in the same fatigue condition. Actually, on the 1/8 of width section surface (Fig. 8c), there are only discontinuous boundary cracks appearing between the 0° and outer 45° plies.

3.2. T800/5245 laminate

Fig. 9a–h show the fatigue-induced damage development recorded by edge replication on a fatigue test sample which was subjected to repeated tension cycling at a maximum stress of 80% of the tensile strength. Fig. 9a shows the original condition of the sample before being cyclically loaded, and Fig. 9b gives an enlarged view of the original fibre condition. Apart from a poor surface condition, there is no visible evidence of progressive damage in these two photos. It must be mentioned that some clean peeling cracks in the surface layers of the skin 45° ply were difficult to avoid in almost all of the test coupons cut from the autoclaved 1 m by 0.3 m plates. This kind of peeling crack in the skin ply was not seen in the XAS/914

Figure 2 Damage conditions at the edge of an XAS/914 $[(\pm 45, 0_2)_2]_s$ specimen subjected to fatigue at a maximum stress of 94% of the strength. (a) Matrix crack in outer 45° plies, $N = 301$. (b) Fibre breakage in 0° plies, $N = 301$. (c) Matrix cracking in inner 45° plies, $N = 2512$. (d) Fibres in 0° plies drop out from edge of sample, $N = 6846$. (e) Detail of fibre drop-out from edges, $N = 6846$. (f) Delamination between $\pm 45°$ plies start from all sample edge, $N = 13000$. (g) Delamination between 0° and 45° plies, $N = 80012$. (h) Formation of small edge delamination between 0° and 45° plies, $N = 80012$. (i) Some fibre fractures in a 0° ply are triggered by an approaching matrix crack in a neighbouring 45° ply, $N = 80012$. (j) The last replica of this specimen after 554 440 cycles.

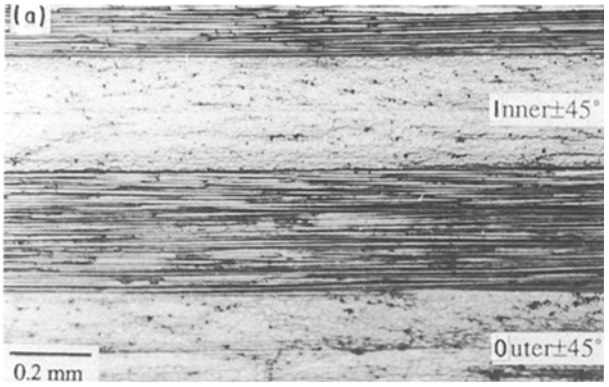

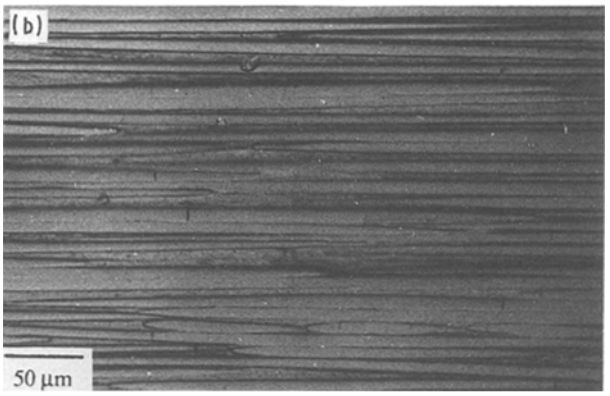

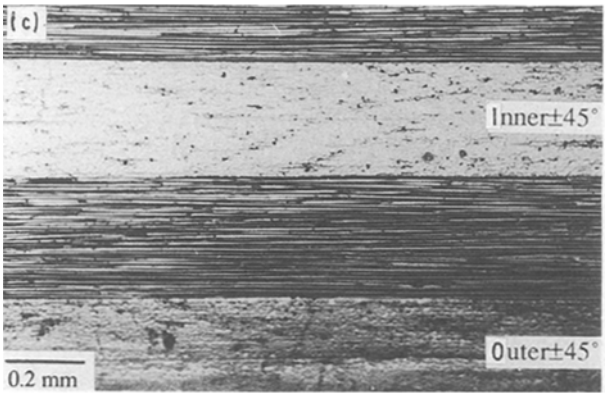

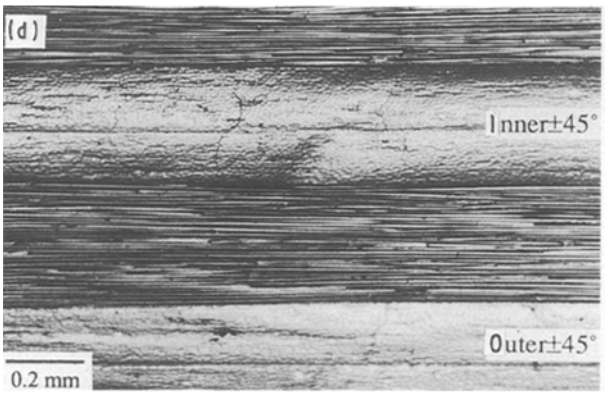

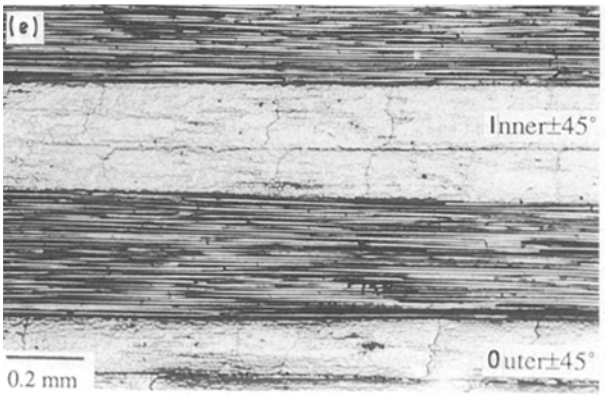

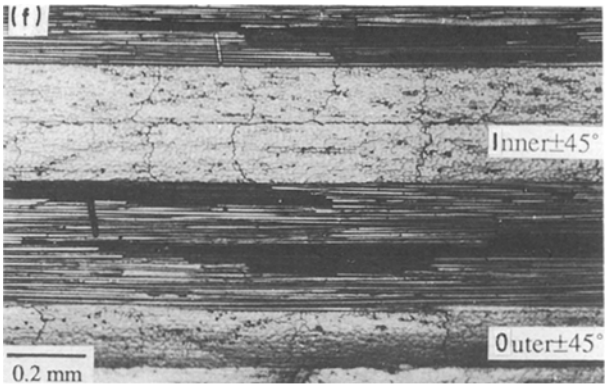

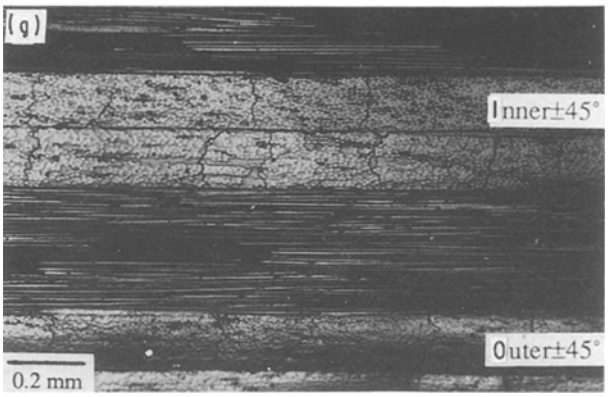

Figure 3 Damage conditions at the edge of an XAS/914 $[(\pm 45, 0_2)_2]_s$ specimen subjected to fatigue at a maximum stress of 78% of the strength. (a) Matrix crack in outer 45° plies, $N = 8499$. (b) Fibre breakage in 0° plies, $N = 8499$. (c) Matrix crack in an inner 45° ply, $N = 37\ 002$. (d) Fibre drop-out from 0° plies, $N = 80\ 042$. (e) Delamination between $\pm 45°$ plies, $N = 160\ 082$. (f) Small delamination between 0° and 45° plies, $N = 450\,056$. (g) The last replica of this specimen, $N = 962\,496$.

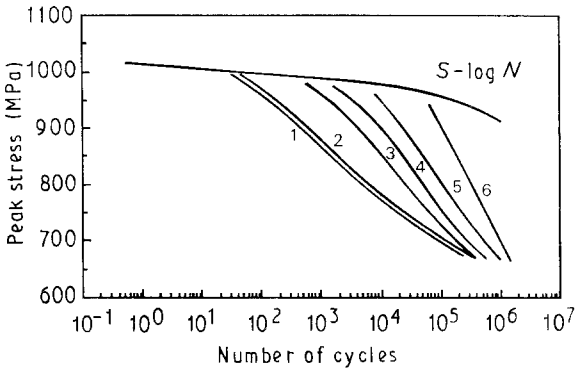

Figure 4 A schematic map of fatigue damage mechanisms for an XAS/914 $[(\pm 45, 0_2)_2]_s$ laminate, $R = 0.1$. 1, Outer matrix crack; 2, fibre fracture; 3, inner matrix crack; 4, fibre drop out; 5, delamination between 45°; 6, delamination between 0° and 45°.

laminates. They might have occurred during the cutting of test samples or may have been inherent, following laminate cure. Nevertheless, no attempt has been made to look into and discuss this matter, because it is beyond the scope of this study. The first fatigue replica of this sample was taken at 58 cycles (Fig. 9c) and some fibre fractures in the 0° plies as well as matrix cracks in the outer $\pm 45°$ plies can be seen as the first signs of recognizable damage: we note that the matrix crack in the skin ply started from a peeling crack already existing in the ply. Fig. 9d gives a view of a

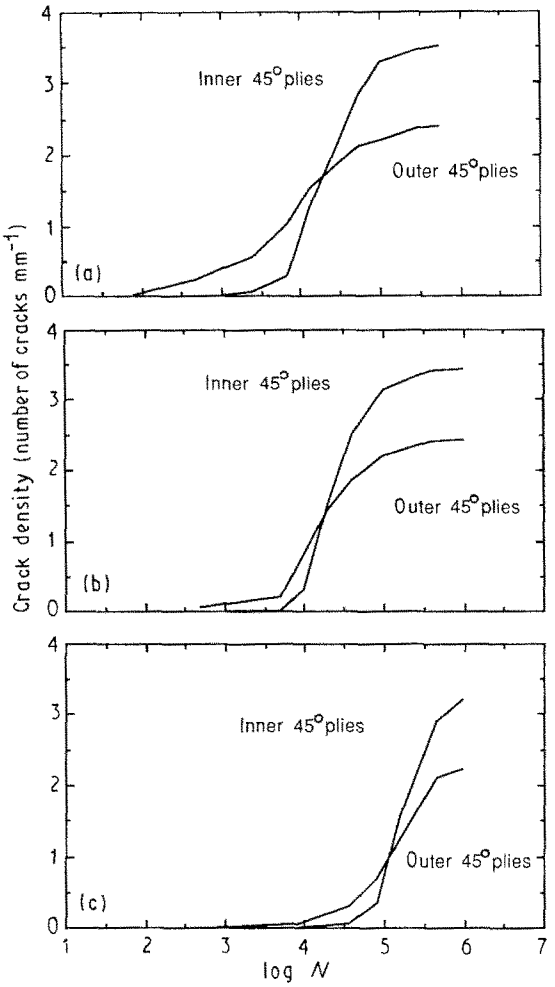

Figure 5 Change of matrix crack density on the edges of XAS/914 $[(\pm 45, 0_2)_2]_s$ samples as a function of fatigue cycles. The specimens are fatigued at different maximum cyclic stresses of (a) 94%, (b) 86% and (c) 78% of the tensile strength.

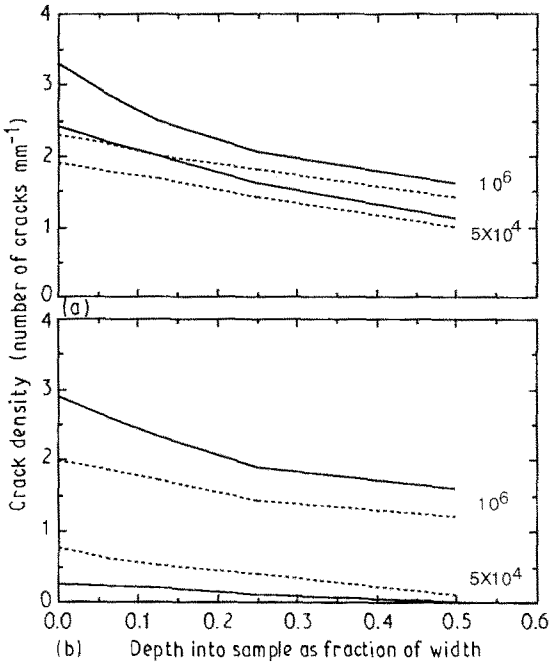

Figure 6 Matrix crack densities as a function of the distance from the edges of XAS/914 $[(\pm 45, 0_2)_2]_s$ specimens fatigued to 5×10^4 and 10^6 cycles at peak stresses of (a) 86% and (b) 75% of the tensile strength. (———) inner 45° plies, (– – –) outer 45° plies.

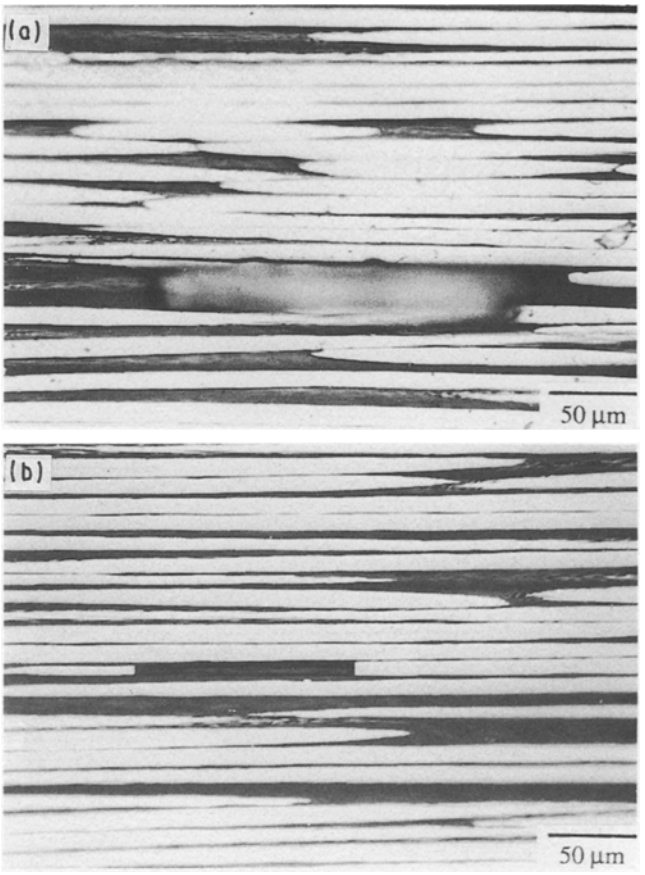

Figure 7 Fibre drop-out from half-width-section surfaces of the XAS/914 $[(\pm 45, 0_2)_2]_s$ samples fatigued to 10^6 cycles at (a) 86% and (b) 75% of the tensile strength.

fibre fracture at higher magnification. After 262 cycles (Fig. 9e), further matrix cracks had occurred in the outer $\pm 45°$ plies, and by contrast to what happened in the XAS/914 laminate specimens, the next damage mechanism observed in this sample, instead of matrix cracking in the inner $\pm 45°$ plies, is fibre drop-out from 0° plies. After about 1000 cycles (Fig. 9f) there is still no sign of matrix cracks in the inner 45° plies. At the same time matrix cracks in the outer 45° plies had triggered some edge delamination between the 0° and 45° plies. Matrix cracks appeared in the inner 45° plies after 2371 cycles (Fig. 9g), and these matrix cracks triggered more small edge delaminations between 0° and $\pm 45°$ plies (Fig. 9h). This sample failed as a result of fatigue after a further 23 679 cycles.

Fig. 10a–h show the damage development in another sample fatigued at a peak stress of 61% of the tensile strength. Fig. 10a gives a view of the original condition. Fibre fracture can be seen in the first replica taken at 60 cycles (Fig. 10b) even though the cumulative number of fibre fractures is clearly less than in samples fatigued at higher stress levels for a similar number of cycles (Fig. 9d). At this stage, matrix cracks have not occurred in the outer $\pm 45°$ plies (Fig. 10c). The first matrix crack in a skin 45° ply can be seen at about 400 cycles (Fig. 10d). Further matrix cracks occurred in the outer $\pm 45°$ plies with continued cycling (Fig. 10e). By this stage, about 20 000 cycles, no sign of matrix cracking in the inner $\pm 45°$ plies can be

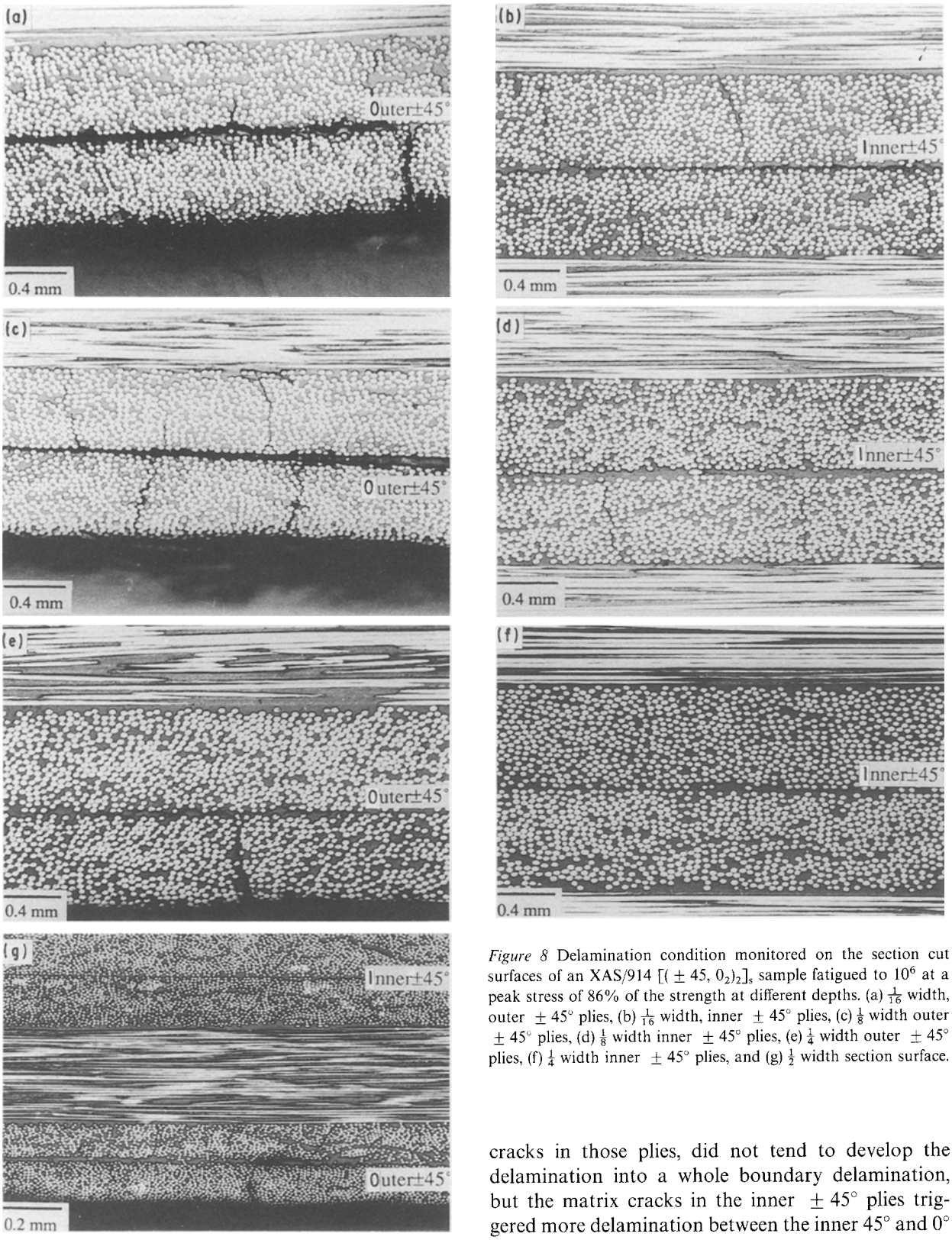

Figure 8 Delamination condition monitored on the section cut surfaces of an XAS/914 $[(\pm 45, 0_2)_2]_s$ sample fatigued to 10^6 at a peak stress of 86% of the strength at different depths. (a) $\frac{1}{16}$ width, outer $\pm 45°$ plies, (b) $\frac{1}{16}$ width, inner $\pm 45°$ plies, (c) $\frac{1}{8}$ width outer $\pm 45°$ plies, (d) $\frac{1}{8}$ width inner $\pm 45°$ plies, (e) $\frac{1}{4}$ width outer $\pm 45°$ plies, (f) $\frac{1}{4}$ width inner $\pm 45°$ plies, and (g) $\frac{1}{2}$ width section surface.

observed, but fibre drop-out from the 0° plies has occurred. Matrix cracks formed in the inner $\pm 45°$ plies at about 120 000 cycles in this sample (Fig. 10f). Fig. 10g shows the fatigue damage condition after 1073 031 cycles: this sample did not fail in fatigue and the test was stopped. The number of matrix cracks in the inner $\pm 45°$ plies has increased. The small edge delamination between the two adjacent $\pm 45°$ plies, which is introduced by the two closely spaced matrix cracks in those plies, did not tend to develop the delamination into a whole boundary delamination, but the matrix cracks in the inner $\pm 45°$ plies triggered more delamination between the inner 45° and 0° plies (Fig. 10h).

The microscopic damage state study based on the edge replicas was carried out in a fatigue stress range in which maximum stress varied from 50%–90% of the monotonic tensile strength for eight samples. As in the case of the XAS/914 composite, a schematic map of damage mechanisms for the T800/5245 $[(\pm 45, 0_2)_2]_s$ material can be plotted in terms of peak fatigue stress versus logarithmic number of cycles (Fig. 11) on the basis of the information obtained from edge replication. As mentioned previously, although fibre fracture can be seen in all of the early replicas after about

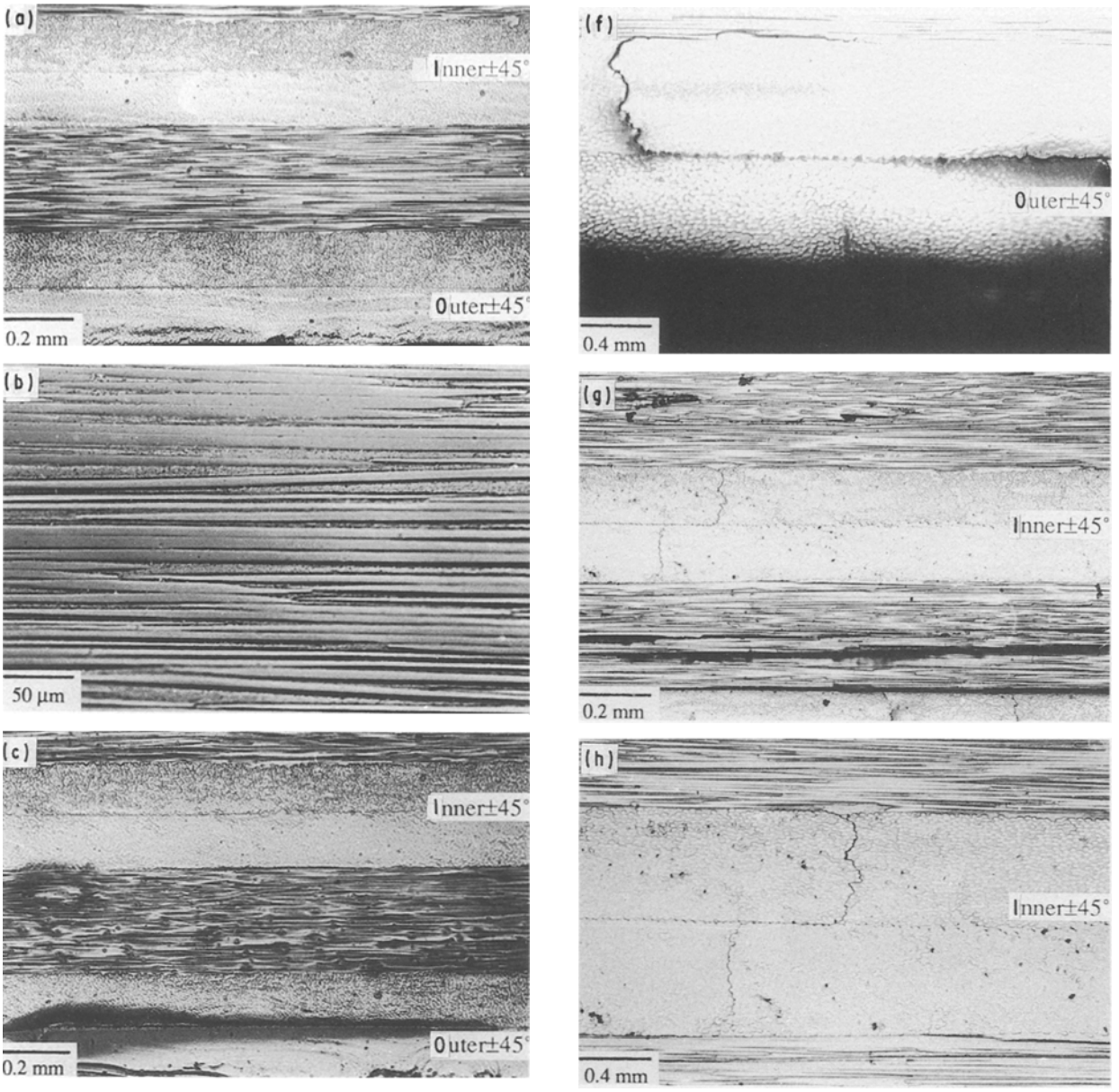

Figure 9 Fatigue damage condition on the edge of a T800/5245 $[(\pm 45, 0_2)_2]_s$ specimen subjected to fatigue at a maximum stress of 80% of the strength. (a) The original condition. (b) A close view of the original fibre condition. (c) Matrix cracking in outer 45° plies and fibre fracture in 0° plies, $N = 58$. (d) Fibre fractures in 0° plies, $N = 58$. (e) fibre drop-out from 0° plies and more matrix cracks in outer 45° plies, but no sign of matrix cracking in inner 45° plies, $N = 262$. (f) Matrix cracks triggered small edge delamination between 0° and 45° plies, $N = 1000$. (g) Matrix cracking in inner 45° plies, $N = 2371$. (h) Small delamination between 0° and 45° plies triggered by matrix cracks in inner 45° plies, $N = 2371$.

50–60 cycles, the numbers of fibre fractures are clearly greater at higher stress levels. Given that we have relatively little accurate information about the threshold for fibre fracture, because no replicas could be taken within the first few tens of cycles, the damage curve for fibre fracture in Fig. 11 could reasonably be corrected to a position given by the line furthest to the left.

3.3. Examination of fatigue fracture surfaces with SEM

Fig. 12a shows a scanning electron micrograph of the fracture surface of a T800/5245 $[(\pm 45, 0_2)_2]_s$ sample

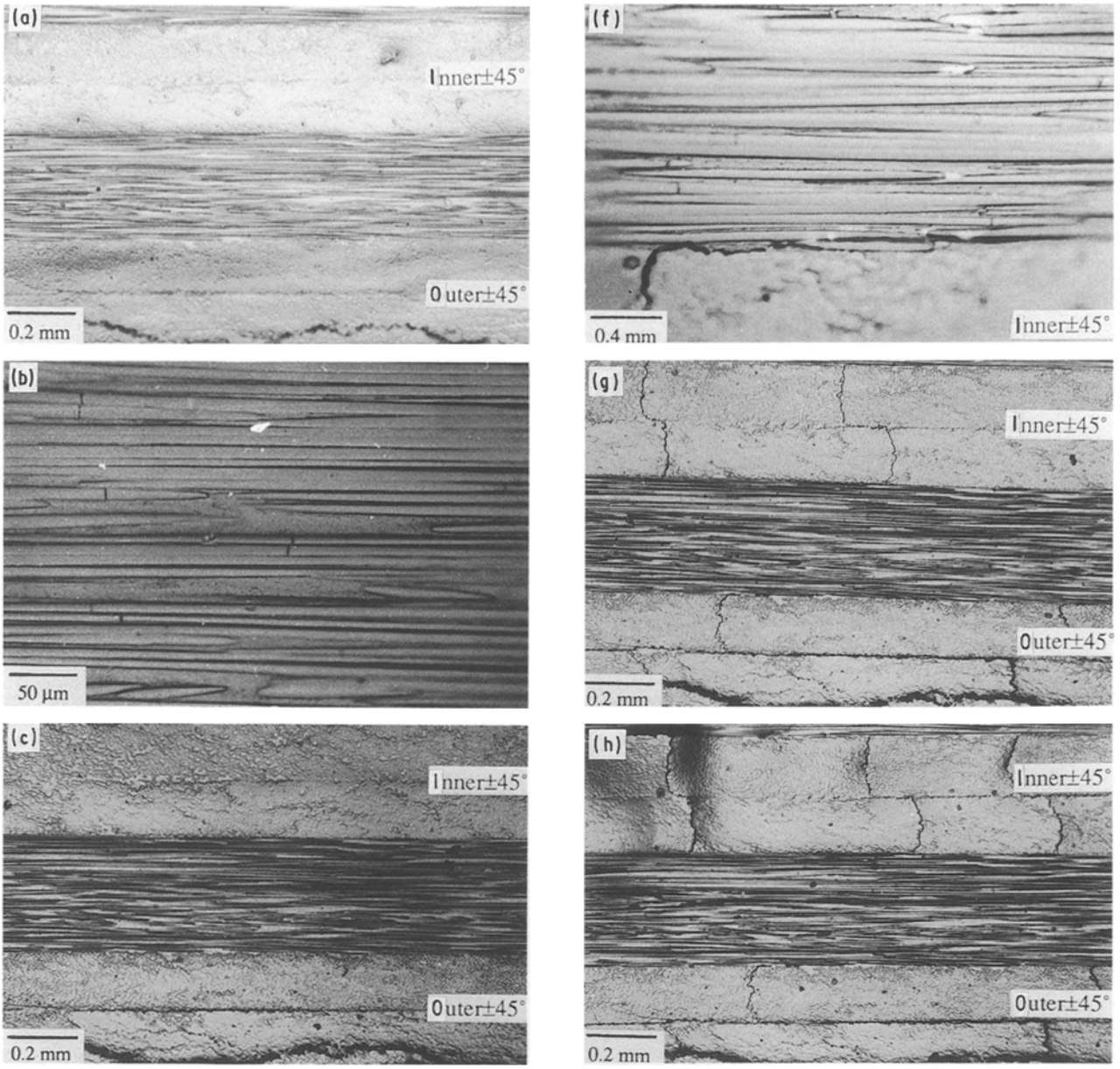

Figure 10 Fatigue damage condition on the edge of a T800/5245 $[(\pm 45, 0_2)_2]_s$ specimen subjected to fatigue at a maximum stress of 61% of the tensile strength, (a) The original condition. (b) Fibre fractures, $N = 60$. (c) No matrix crack in outer 45° plies, $N = 60$. (d) Matrix crack in an outer 45° ply, $N = 400$. (e) No matrix crack in inner 45° plies, but fibre drop-out from 0° plies, $N = 20\,000$. (f) Matrix crack in inner 45° plies, $N = 120\,000$. (g) Last replica of this sample, $N = 1173\,031$. (h) Small delamination triggered by inner 45° matrix crack between 0° and 45° plies, the last replica.

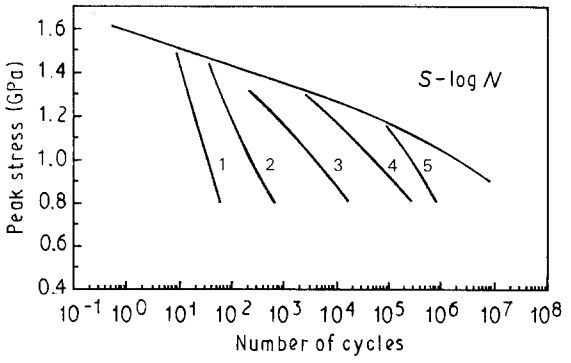

Figure 11 A schematic map of the fatigue-induced damage mechanisms for T800/5245 $[(\pm 45, 0_2)_2]_s$ laminate, $R = 0.1$. 1, Fibre fracture; 2, outer matrix crack; 3, fibre drop-out; 4, inner matrix crack; 5, delamination between 45° and 0°.

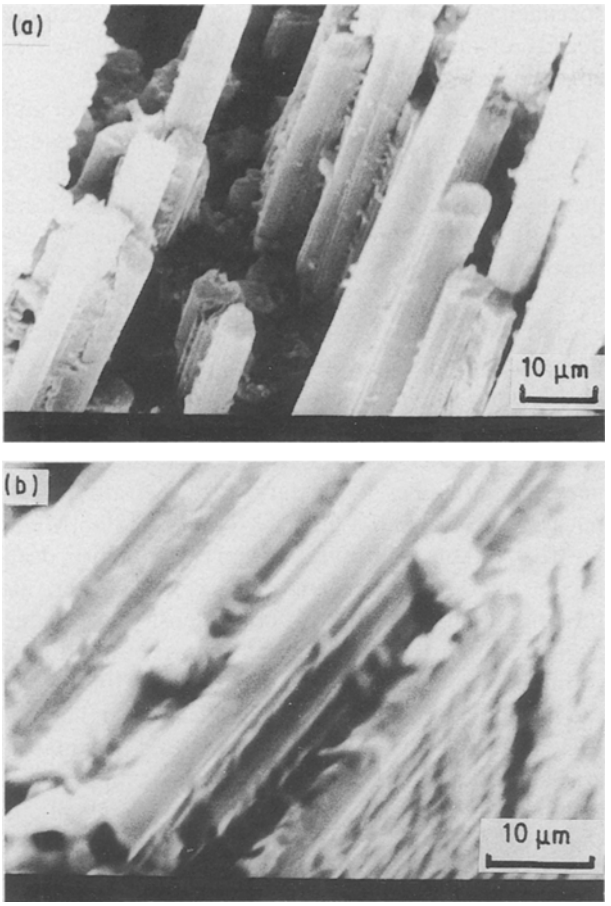

Figure 12 Scanning electron micrographs of fatigue fracture surfaces of a T800/5245 $[(\pm 45, 0_2)_2]_s$ specimen subjected to maximum cyclic stress = 1.20 GPa, and failed at about 2×10^4 cycles. The views are focused on (a) 0° plies area, (b) 45° plies area.

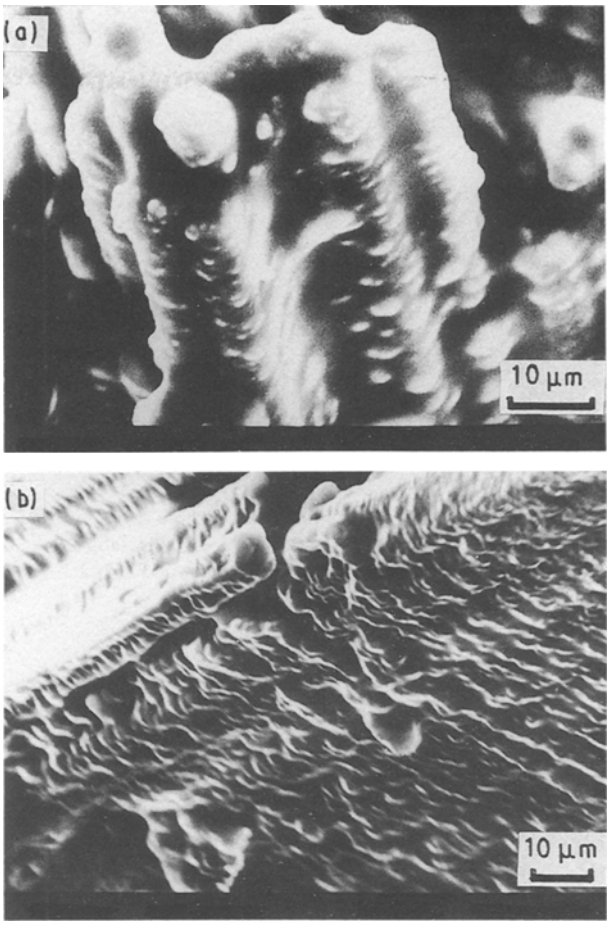

Figure 13 Scanning electron micrographs of fatigue fracture surfaces of an XAS/914 $[(\pm 45, 0_2)_2]_s$ specimen subjected to a maximum cyclic stress = 0.92 GPa, and failed at about 4×10^5 cycles. The views are focused on (a) 0° plies area, (b) 45° plies area.

which failed during fatigue at a maximum cyclic stress of 1.20 GPa (about 75% of the tensile strength) after about 20 000 cycles. This is a view focused on a 0° ply area of the fracture surface. The failure mechanism of fibre pull-out can be seen very clearly, and almost all of the fibre surfaces are free of residual matrix resin as a consequence of clean debonding at the fibre/matrix interface. By contrast, SEM observations of the fatigue fracture surface of the XAS/914 laminate show a very different situation. Fig. 13a is an SEM view of the fatigue fracture surface of an XAS/914 $[(\pm 45, 0_2)_2]_s$ sample which failed during fatigue at a 0.92 GPa maximum stress (about 91.5% of the tensile strength) after about 400 000 cycles. This view is again focused on a 0° ply area of the fracture surface, and the magnification is the same as for the Fig. 12a. An obviously different failure mode from the one presented in Fig. 12a is very clearly seen. Even after final fracture, most of the fibres in the 0° plies are still stuck together, and the matrix resin adheres to the fibre surfaces. No single clean fibre surface can be seen here. Actually, similar examples of these sharp distinct failure modes have been observed in fibre drop-out phenomena from the edges of the 0° plies of the two material system specimens. Interfibre splitting in the XAS/914 composite occurred in the matrix resin and the fibres which subsequently dropped out are well covered by the matrix resin (Fig. 14), whereas the

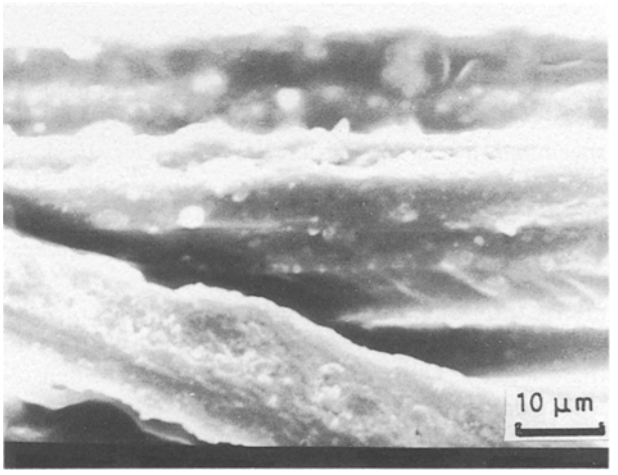

Figure 14 Scanning electron micrograph of fibre drop-out from the edge of an XAS/914 $[(\pm 45, 0_2)_2]_s$ specimen fatigued at a maximum stress of 75% of the strength to about 10^5 cycles.

interfibre splitting in the T800/5245 composite occurred as a result of debonding at the fibre/matrix interface (Fig. 15). In this case the fibre is so free of residual matrix resin that scratches on the fibre surface can be clearly seen. Fig. 12b and 13b show views focused on the 45° ply areas of the fatigue fracture surfaces of the same specimens as in Fig. 12a and 13a, respectively.

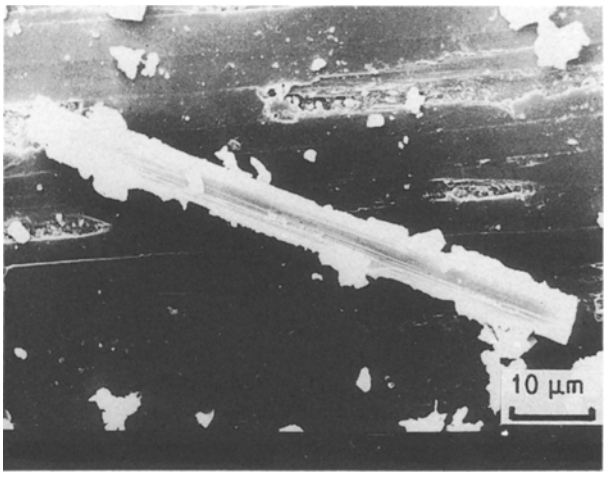

Figure 15 Scanning electron micrograph of fibre drop-out from a free edge of a T800/5245 $[(\pm 45, 0_2)_2]_s$ sample fatigued at a maximum stress of 70% of the strength to about 10^4 cycles.

The lower right-hand corners of the photos are areas of delamination between the 45° plies and 0° plies. The different failure modes are also presented in these two photos. The surfaces of the T800 fibres are exposed with no matrix resin cover (Fig. 12b), while the XAS fibres are covered with the residual resin (Fig. 13b). In the delamination areas, the residual matrix resin shows that clean interlaminar deformation has occurred in the matrix resin in the XAS/914 material (Fig. 13b). However, the rather flat delamination surface in the T800/5245 material suggests that the delamination in this material occurred in a mode with more fibre/matrix interface cracking than interlaminar matrix cracking (Fig. 12b).

4. Discussion

On the subject of the initiation and development of matrix cracks on the free edges of the XAS/914 system specimens, it was shown that the "characteristic damage state" could be achieved in off-axis plies. The question here, however, is how far these matrix cracks would have grown into the specimen and how representative of the internal CDS the edge replication information might be. The sectioning studies provide an opportunity to investigate the growth features of these cracks. The reduction in matrix crack density with increasing distance from the free edge indicates that under the over-all repeated uniform tensile stress or strain, the stress/strain condition through the sample width is not uniform. There is a strong influence of free-edge effects on the axial stress/strain distribution which allows the matrix cracks to initiate and grow in the 45° plies mainly in a Mode I fashion. This may occur as a result of the familiar increase in interlaminar shear stress near the edges of a sample loaded in tension [32]. The matrix cracks initiated at the edges as a consequence of the free-edge effect could not easily grow deep into the samples in this condition. Therefore, the CDS at the free edge should be the worst damage condition in the whole specimen, and could not be a true representation of the bulk of the specimen unless a reasonable relationship between the density of matrix cracks and distance from the free edge can be verified.

The difference in the crack densities in the inner and outer $\pm 45°$ plies on the edge of a cyclically loaded specimen, as shown in Fig. 5, could be a result of the fact that the outer 45° plies were easy to separate from the rest of the laminate and would then lose the capability of bearing load. Being less rigidly bounded by 0° plies allows the outer $\pm 45°$ plies to separate easily from the whole laminate structure. This means that the delaminations between adjacent $\pm 45°$ layers in the outer plies and between the outer 45° plies and 0° plies are more likely to form once matrix cracks occur in the outer 45° plies, because that delamination near the skin plies has a larger total strain energy release rate [33] and a higher Mode I-to-total (Mode I + II + III) mechanism ratio than delamination deep in the interior of the laminate [34]. However, although initially the outer-ply crack density at the edge is greater than that in the inner plies, the situation is soon reversed and for fatigue beyond a certain stage the inner ply crack density is significantly higher, see Fig. 5. For a delamination introduced by matrix cracks in the skin 45° plies, the physical consequence of the delamination is that a piece of 45° ply is separated from the whole laminate body and loses its load-bearing function so that no further stress can be put on it [35]. With this kind of process going on, the scope for matrix cracking in the outer 45° plies will certainly be reduced so as to obtain the lower matrix crack density.

It is noted that fibre drop-out from edges occurs in a particular range of the fatigue life at different cyclic load levels for both laminates (Figs 4 and 11), so that it has been identified as a specific fatigue damage mechanism. The fibre drop-out could be the physical consequence of a piece of fibre or a group of fibres being isolated by the combined effects of a fibre fracture and subsequent splitting between fibres. When the laminate samples are subjected to a uniform axial tensile stress, it is expected that fibre breakage will readily spread into all 0° plies [36]. The transverse and shear stress concentrations near the tip of a fibre break would initiate a split in the plies along the direction of the fibre orientation [37], following which, the isolated fragment could peel away from the edge surface as schematically illustrated in Fig. 16. With further cyclic loading, fibres will continue to peel away from the newly exposed edge surface in this fashion. Because fibre breakage can occur anywhere in the load-bearing 0° plies, fibre drop-outs are expected to be observed in any exposed layer parallel to the fibre orientation in the 0° plies. The observation of fibre drop-out in the sectioned surfaces of some XAS/914 specimens provides strong evidence (Fig. 7a and b) that the drop-out phenomenon is a bulk failure mechanism, not merely a free-edge effect. The splitting parallel to the fibre orientation would not necessarily be a result of debonding between the fibres and the surrounding matrix resin. This interfibre fracture could well be a matrix crack parallel to the fibre orientation direction if the bond strength between

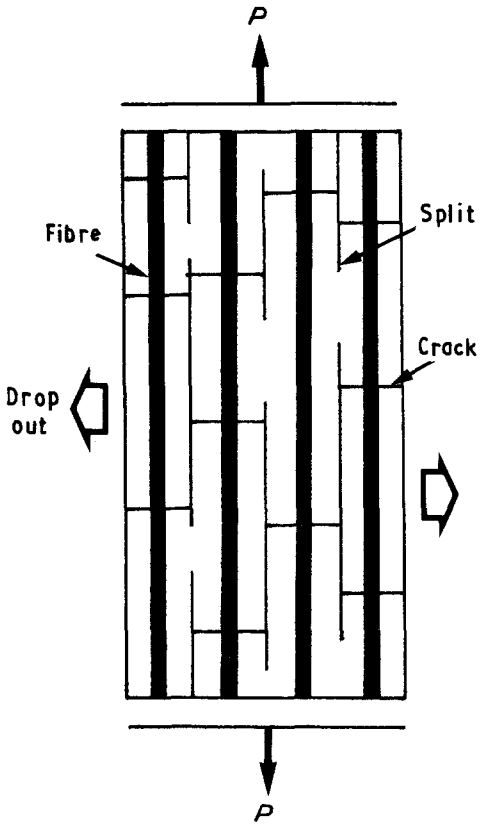

Figure 16 Illustration of fibre drop-out from the edge of a 0° ply as a result of fibre breakage and interfibre splitting.

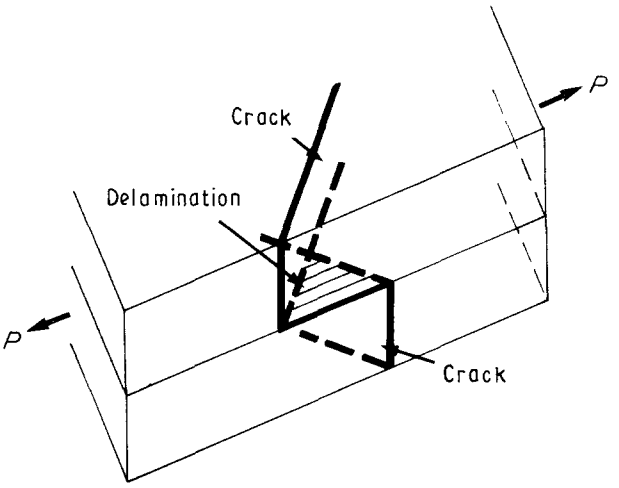

Figure 17 Illustration of delamination between ± 45° plies as the result of two matrix cracks in adjacent ± 45°s.

fibre and matrix resin is higher than the strength of the matrix resin. Scanning electronic microscope (SEM) studies of fibre drop-out have shown the difference in the inter-fibre fracture modes of these two materials. The split in the XAS/914 system visible in Fig. 14 had occurred in the matrix resin. But in the T800/5245 material the low strength of the fibre/matrix interface allows splitting to occur as a result of debonding between fibre and matrix (Fig. 15).

Delamination is one of the most important fatigue damage mechanisms in composite laminates. As previously discussed in relation to damage observation with edge replicas of the XAS/914 material, delamination between adjacent ± 45° plies is apparently the extension of small edge interlaminar matrix cracks between two in-ply matrix cracks in the two plies as shown schematically in Fig. 17. Under the influence of the free-edge effect, growth along the load axis of these small edge delaminations during fatigue is expected to occur mostly near the edges. In addition to the interlaminar normal and shear stresses from the free-edge effect, the interlaminar shear stress caused by the two in-ply cracks enables this interlaminar matrix crack to grow, mainly in Modes I and II, soon after the formation of the in-ply matrix cracks. The delamination of the whole boundary of ± 45° plies on the edges of XAS/914 specimens can occur at a certain stage of the fatigue as a result of this growth. The delamination between 0° and 45° plies of the XAS/914 laminate, observed in the edge replicas and sectioned surfaces, starts later and grows much less deeply into the laminate than that between + 45° and − 45° plies in the same fatigue condition. This is because a stress concentration normal to the interlaminar boundary of 0° and 45° plies is expected to be smaller than that normal to the ± 45° as a result of the fact that the difference between the configurations on either side of this boundary is not as large as those on the ± 45° boundary.

By contrast with the XAS/914 material, in the T800/5245 laminate the whole boundary edge delamination damage occurs first between 0° and 45° plies. Although a small edge delamination between two adjacent ± 45° plies could initiate under the strong shear stress condition created by the two matrix cracks formed in the two adjacent ± 45° plies, they are not expected to grow to the whole edge boundary length like those between 0° and 45° plies. The weak interfacial bond strength between T800 fibre and 5245 resin could be the primary reason for this. As has been noted from damage observation on the edge replicas, a small interlaminar crack between 0° and 45° plies could easily be triggered by an approaching matrix crack in the adjacent 45° ply. This interlaminar crack, formed mainly in the weak fibre/matrix boundary, together with the interfibre debond splitting caused by fibre fracture and the weak interfacial strength of the load-bearing 0° plies, could act jointly to separate 0° plies from 45° plies.

The SEM observations indicate that the interfacial shear strength (IFSS) of the T800/5245 system is much lower than that of the XAS/914 system, even though the strength of both the T800 fibres and the 5245 resin are higher than their counterparts in the XAS/914 system. It is understood that the different IFSS levels of the two materials is a main reason for the different appearances of the fatigue-induced damage mechanisms and the different over-all fatigue performances of the two materials. Under an external tensile load, the low interfacial shear strength of the T800/5245 could allow debonding to occur between fibre and matrix resin as a result of the induced shear stress pulse immediately after a fibre fracture occurred [38]. A stress concentration could be introduced into neighbouring fibres as a consequence of the fact that the nearby debonded fibre no longer carries any load, and

this will lead to further fibre fracture and debonding during further loading. A repeated tension load could accelerate the above process by means of a physically repeated crack opening/closing mechanism so that the T800/5245 composite exhibits poor fatigue performance. By contrast with the T800/5245, the higher interfacial shear strength of the XAS/914 fibre/matrix bond could allow fibres to contribute their load-carrying ability until they have been broken (because of the different strain limit in the surrounding matrix resin) to a specific small length which is no longer sufficient to provide adequate shear transfer through the fibre/matrix interface [39, 40]. In this high IFSS composite, the load-carrying ability of fibres could be affected by the strength of the matrix resin. The failure mode here is interfibre rather than interfacial, because the stress transfer is limited by shear yielding of the matrix resin and not by the failure of the fibre/matrix interface bonding [41].

Following the above observations and discussion, a reasonably clear picture of the fatigue damage mechanisms in the XAS/914 and T800/5245 $[(\pm 45, 0_2)_2]_s$ laminates in the given cyclic loading conditions has been obtained. Although the well-known damage mechanisms of fibre-reinforced plastic composites, such as fibre breakage, matrix cracking, delamination and debonding, have all been involved, the order and forms of these damage mechanisms in the fatigue condition can be recognized as being characteristically different for different materials. The tendency of almost all of the damage mechanisms occurring in the laminate under the influence of the free-edge effect to be edge-related, indicates that the damage situation deep inside the laminates cannot be worse than the damage state on the free edges. On the basis of this estimation, the damage mechanisms outlined in the schematic damage maps shown in Figs 4 and 11, can be regarded as prior information of the damage states for these materials in the given fatigue conditions.

Apart from the orders of the different damage onset curves, the shapes of these damage curves in the maps can also indicate the different fatigue performances of the two composite materials. The damage onset curves of the XAS/914 material have shown that there is possibly a fatigue stress limit at about 60% of the tensile strength, below which no damage will occur under fatigue conditions (Fig. 4). However, this kind of fatigue limit for the occurrence of damage does not appear for the T800/5245 material, even at fatigue stresses as low as 50% of the tensile strength (Fig. 11). It is noted that the shapes of the damage mechanism curves in the maps can only be determined to within a limited degree of accuracy unless the cyclic loading tests are stopped at inconveniently short intervals. Nevertheless, the shapes of the damage curves and their relationship with established parts of the $S/\log N$ curves of these materials suggest that the final fatigue fracture which $S/\log N$ curves indicate could probably be treated as the last ultimate damage onset stage. Therefore, the remaining regions of the $S/\log N$ curves ($N > 10^6$), which cannot be determined in a reasonable experimental time scale, could follow the same change tendencies as the damage curves of the material. Some preliminary work has been carried out on the concept of predicting the $S/\log N$ curve by modelling of the damage curves [42].

5. Conclusions

It was the intention of this work to investigate the damage condition development during tension–tension constant amplitude fatigue cycling of two carbon-fibre/epoxy systems, namely XAS/914 and T800/5245 in $[(\pm 45, 0_2)_2]_s$ lay-ups. The conclusions of this work can be summarized as follows.

1. Several damage mechanisms, including matrix cracking, fibre fracture, delamination and fibre end drop-out from the edges of the 0° plies (or in isolation inside the plies as a combination of fibre fracture and interfibre splitting) have been observed during fatigue. They appeared in distinctive manner and order in the two composite materials.

2. All of the damage mechanisms occur in a specific sequence at different numbers of cycles according to the fatigue stress levels, and this sequence can be changed in composite systems which have different structural properties, such as fibre/matrix interfacial bond strength. The damage maps, which combine all fatigue-induced damage information, can be recognized as characteristic of different composite material systems.

3. The fatigue resistance of the XAS/914 $[(\pm 45, 0_2)_2]_s$, in terms of fatigue-induced damage condition under tension–tension cyclic loading, is superior to that of T800/5245 laminate of the same lay-up, even though the latter material has a higher monotonic tensile strength than the former.

4. The poorer fatigue performance of the T800/5245 material may be due to its low fibre/matrix interfacial bond strength which allows fibre-related damage to occur easily in the 0° plies, thus reducing the fatigue resistance of the whole laminate.

Acknowledgement

A.S. Chen thanks the British Council for financial support during his research programme at the University of Bath.

References

1. B. HARRIS, "Engineering Composite Materials" (The Institute of Metals, London, 1986).
2. K. L. REIFSNIDER, in "Proceedings of ICCM/6 and ECCM/2", London, edited by F. L. Matthews N. C. R. Buskell, J. M. Hodgkinsen and J. Morton (Elsevier Applied Science, London, 1987) p. 4.1.
3. T. K. O'BRIEN, G. B. MURRI and S. A. SALPEKAR, ASTM STP 1012 (American Society for Testing and Materials, Philadelphia, PA, 1989) pp. 222–50.
4. T. K. O'BRIEN, "Towards a Damage Tolerance Philosophy for Composite Materials and Structures," NASA Technical Memorandum 100548 (March 1988).
5. A. ROTEM, and Z. HASHIN, *AIAA J.* **14** (1976) 868.
6. A. ROTEM, *ibid.* **17** (1979) 271.
7. LIN YE, *Comp. Sci. Tech.* **33** (1988) 257.
8. J. ABOUDI, *J. Reinf. Plastics Compos.* **18** (1989) 150.
9. T. ADAM, G. FERNANDO, R. F. DICKSON, H. REITER and B. HARRIS, *Int. J. Fatigue* **10** (1989) 233.

10. T. ADAM, R. F. DICKSON, C. JONES, H. REITER and B. HARRIS, *Proc. Inst. Mech Eng.* **200** (1986) 155.
11. H. A. WEITWORTH, *J. Compos. Mater.* **21** (1987) 311.
12. A. ROTEM, *J. Compos. Technol. Res.* **11** (1989) 59.
13. W. HWANG and K. S. HAN, *J. Compos. Mater.* **20** (1986) 154.
14. J. N. YANG and M. D. LIU, *ibid.* **11** (1977) 176.
15. J. N. YANG, *ibid.* **12** (1978) 19.
16. A. ROTEM, *Int. J. Fatigue* **9** (1988) 27.
17. K. L. REIFSNIDER and A. HIGHSMITH, in "Materials Experimentation and Design in Fatigue" (Butterworths Scientific Ltd., Westbury House, UK 1981) pp. 246–60.
18. K. L. REIFSNIDER and A. TALUY, *Int. J. Fatigue* **5** (1983) 3.
19. A. L. HIGHSMITH and K. L. REIFSNIDER, ASTM STP 775 (American Society for Testing and Materials, Philadelphia, PA, 1982) pp. 103–17.
20. S. L. OGIN, P. A. SMITH and P. W. R. BEAUMONT, *Compos. Sci. Tech.* **22** (1985) 23.
21. A. POUSRARTIP, M. F. ASHBY and P. W. R. BEAUMONT, *ibid.* **25** (1986) 173.
22. P. S. STEIF, *J. Compos. Mater.* **17** (1984) 153.
23. A. L. HIGHSMITH, W. W. STINCHCOMB and K. L. REIFSNIDER, ASTM STP 836 (American Society for Testing and Materials, Philadelphia, PA, 1984) pp. 194–216.
24. K. L. REIFSNIDER, W. W. STINCHCOMB and T. K. O'BRIEN, ASTM STP 636 (American Society for Testing and Materials, Philadelphia, PA, 1977) pp. 171–84.
25. W. W. STINCHCOMB and K. L. REIFSNIDER, ASTM STP 675 (American Society for Testing and Materials, Philadelphia, PA, 1979) pp. 762–81.
26. G. C. TSAI, J. F. DOYLE and C. T. SUN, *J. Compos. Mater.* **21** (1987) 2.
27. D. C. CURTIS, D. R. MOORE, B. SLATER and N. ZAHLAN, *Composites* **19** (1988) 446.
28. C. J. JONES, R. F. DICKSON, T. ADAM, H. REITER and B. HARRIS, *Proc. R. Soc.* **A396** (1984) 315.
29. R. F. DICKSON, C. J. JONES, B. HARRIS, D. C. LEACH and D. R. MOORE, *J. Mater. Sci.* **20** (1985) 60.
30. J. M. WHITNEY, ASTM STP 521 (American Society for Testing and Materials, Philadelphia, PA, 1973) pp. 167–80.
31. N. J. PAGANO and R. B. PIPES, *Int. J. Mech. Sci.* **15** (1973) 679.
32. E. D. REEDY Jr, *Compos. Sci. Tech.* **34** (1989) 259.
33. T. K. O'BRIEN, ASTM STP 775 (American Society for Testing and Materials, Philadelphia, PA, 1982) pp. 140–67.
34. J. D. WHITCOMB and I. S. RAJU, ASTM STP 876 (American Society for Testing and Materials, Philadelphia, PA, 1985) pp. 69–94.
35. M. D. THOULESS, H. C. CAO and P. A. MATAGA, *J. Mater. Sci.* **24** (1989) 1406.
36. L. LORENZO and H. T. HAHN, ASTM STP 907 (American Society for Testing and Materials, Philadelphia, PA, 1986) pp. 201–32.
37. A. C. GRAG, *Eng. Fract. Mech.* **24** (1986) 255.
38. A. N. NETRAVALI, R. B. HENSTENBURG, S. L. PHOENIX and P. SCHWARTZ, *Composites* **10** (1989) 226.
39. L. T. DRZAL, M. J. RICH and P. LLOYD, *J. Adhesion* **16** (1983) 1.
40. L. T. DRZAL, M. J. RICH, M. F. KOENIG and P. LLOYD, *ibid.* **16** (1983) 133.
41. W. D. BASCOM and R. N. JENSEN, *ibid.* **19** (1986) 219.
42. A. S. CHEN, PhD thesis, University of Bath (1991).

Received 3 August
and accepted 12 October 1992